THE MULTIPLICITY OF MASSIVE STARS: A HIGH ANGULAR RESOLUTION SURVEY WITH THE *HST* FINE GUIDANCE SENSOR*

E. J. Aldoretta[1,2], S. M. Caballero-Nieves[3], D. R. Gies[1], E. P. Nelan[4], D. J. Wallace[5,6], W. I. Hartkopf[7], T. J. Henry[1], W.-C. Jao[1], J. Maíz Apellániz[8], B. D. Mason[7], A. F. J. Moffat[2], R. P. Norris[1], N. D. Richardson[2], and S. J. Williams[9]

[1] Center for High Angular Resolution Astronomy, Department of Physics and Astronomy, Georgia State University, P. O. Box 5060, Atlanta, GA 30302-5060, USA; emily@astro.umontreal.ca; gies@chara.gsu.edu; thenry@chara.gsu.edu; jao@chara.gsu.edu; norris@chara.gsu.edu

[2] Département de physique and Centre de Recherche en Astrophysique du Québec (CRAQ), Université de Montreal, CP 6128 Succ. A., Centre-Ville, Montréal, Québec H3C 3J7, Canada; emily@astro.umontreal.ca; moffat@astro.umontreal.ca; richardson@astro.umontreal.ca

[3] Department of Physics and Astronomy, University of Sheffield, Hicks Building, Hounsfield Road, Sheffield, S3 7RH, UK; s.caballero@sheffield.ac.uk

[4] Space Telescope Science Institute, 3700 San Martin Drive, Baltimore, MD 21218, USA; nelan@stsci.edu

[5] Department of Natural Science, University of South Carolina—Beaufort, 801 Carteret Street, Beaufort, SC 29902, USA; debra.j.wallace@nasa.gov

[6] NASA, Astrophysics Division, 300 E Street, SW, Washington, DC 20546-0001, USA

[7] US Naval Observatory, Astrometry Department, 3450 Massachusetts Avenue NW, Washington, DC 20392-5420, USA; william.hartkopf@usno.navy.mil; brian.mason@usno.navy.mil

[8] Instituto de Astrofísica de Andalucía—CSIC, Glorieta de la Astronomía, s/n. E-18008, Granada, Spain; jmaiz@iaa.es

[9] Institute for Astronomy, Astrophysics, Space Applications and Remote Sensing (IAASARS), National Observatory of Athens, I. Metaxa & Vas. Pavlou Street, Palea Penteli, 15236 Athens, Greece; williams@astro.noa.gr

Received 2014 May 30; accepted 2014 September 3; published 2014 December 19

ABSTRACT

We present the results of an all-sky survey made with the Fine Guidance Sensor on the *Hubble Space Telescope* to search for angularly resolved binary systems among massive stars. The sample of 224 stars is comprised mainly of Galactic O- and B-type stars and luminous blue variables, plus a few luminous stars in the Large Magellanic Cloud. The FGS TRANS mode observations are sensitive to the detection of companions with an angular separation between $0''01$ and $1''0$ and brighter than $\triangle m = 5$. The FGS observations resolved 52 binary and 6 triple star systems and detected partially resolved binaries in 7 additional targets (43 of these are new detections). These numbers yield a companion detection frequency of 29% for the FGS survey. We also gathered literature results on the numbers of close spectroscopic binaries and wider astrometric binaries among the sample, and we present estimates of the frequency of multiple systems and the companion frequency for subsets of stars residing in clusters and associations, field stars, and runaway stars. These results confirm the high multiplicity fraction, especially among massive stars in clusters and associations. We show that the period distribution is approximately flat in increments of log P. We identify a number of systems of potential interest for long-term orbital determinations, and we note the importance of some of these companions for the interpretation of the radial velocities and light curves of close binaries that have third companions.

Key words: binaries: general – stars: early-type – stars: massive – techniques: high angular resolution

Supporting material: figure set, machine-readable and VO tables

1. INTRODUCTION

The formation of a star from a very large natal cloud presents a formidable problem of angular momentum redistribution (Larson 2010). Low-mass stars may accomplish the removal of angular momentum through mass loss coupled with the stellar magnetic field (Matt & Pudritz 2008). However, the situation appears to be different for the formation of massive stars that lack pervasive magnetic fields (Zinnecker & Yorke 2007). These stars may form through disk accretion processes (Krumholz et al. 2009; Kuiper & Yorke 2013) and/or competitive accretion of smaller protostars (Bonnell & Bate 2005; Bonnell & Smith 2011); in both cases, the angular momentum may be deposited into the orbital motion of nearby companion stars (Kratter et al. 2008; Bate 2012). Once formed, the massive binary systems may stand the best chance to survive the many dynamical encounters that likely occur in dense cluster environments (Kaczmarek et al. 2011).

There is ample evidence that the binary and multiple star frequency is remarkably high among massive stars (Duchêne & Kraus 2013). Spectroscopic surveys of Galactic OB stars by Chini et al. (2012), Kobulnicky et al. (2012), Sana et al. (2012), and Sota et al. (2014), and of the Large Magellanic Cloud (LMC) Tarantula Nebula region by Sana et al. (2013b), demonstrate that the binary frequency may be ≈70% for binaries with periods smaller than 3000 days. The incidence of longer period binaries has been explored through speckle interferometry by Mason et al. (1998, 2009), adaptive optics (AO) by Turner et al. (2008) and Close et al. (2012), and Lucky Imaging by Maíz Apellániz (2010) and Peter et al. (2012). These studies also demonstrate the high incidence of binaries and multiples among longer period systems. However, because of the great distances of most massive stars, there still exists a significant observational gap in our knowledge of binaries with periods of years to centuries that have radial velocity variations that are too small to measure or angular separations that are only resolvable with optical long baseline interferometry (Kraus et al. 2009; ten Brummelaar et al. 2011; Sana et al. 2011, 2015). It is critical to fill in this gap with new observations in order to determine the nature of the period

1. REPORT DATE **JAN 2015**	2. REPORT TYPE	3. DATES COVERED **00-00-2015 to 00-00-2015**

4. TITLE AND SUBTITLE	5a. CONTRACT NUMBER
The Multiplicity of Massive Stars: A High Angular Resolution Survey With The HST Fine Guidance Sensor	5b. GRANT NUMBER
	5c. PROGRAM ELEMENT NUMBER

6. AUTHOR(S)	5d. PROJECT NUMBER
	5e. TASK NUMBER
	5f. WORK UNIT NUMBER

7. PERFORMING ORGANIZATION NAME(S) AND ADDRESS(ES) **US Naval Observatory,Astrometry Department,,3450 Massachusetts Avenue NW,,Washington,,DC,20392**	8. PERFORMING ORGANIZATION REPORT NUMBER

9. SPONSORING/MONITORING AGENCY NAME(S) AND ADDRESS(ES)	10. SPONSOR/MONITOR'S ACRONYM(S)
	11. SPONSOR/MONITOR'S REPORT NUMBER(S)

12. DISTRIBUTION/AVAILABILITY STATEMENT **Approved for public release; distribution unlimited**

13. SUPPLEMENTARY NOTES **The Astronomical Journal, 149:26 (14pp), 2015 January**

14. ABSTRACT

15. SUBJECT TERMS

16. SECURITY CLASSIFICATION OF:			17. LIMITATION OF ABSTRACT	18. NUMBER OF PAGES	19a. NAME OF RESPONSIBLE PERSON
a. REPORT **unclassified**	b. ABSTRACT **unclassified**	c. THIS PAGE **unclassified**	**Same as Report (SAR)**	**15**	

distribution and to estimate the total binary frequency (Sana et al. 2013b).

The Fine Guidance Sensor (FGS) on the *Hubble Space Telescope* (*HST*) offers us a particularly attractive means to resolve such close visual binaries for even relatively faint targets (Nelan et al. 2014). The prime FGS1r instrument is capable of resolving binaries as close as 10 milliarcseconds (mas) for stars as faint as $V = 16$ mag. The FGS instrument was used to explore the binary frequency of massive stars in two Galactic environments of special interest, the Carina Association by Nelan et al. (2004, 2010) and the Cyg OB2 association by Caballero-Nieves et al. (2014). In both cases, the binary frequency over the angular range of $0''01-1''0$ was found to be $\approx 22\%$.

Here we describe a new all-sky FGS survey of massive stars that we have made with a number of broad goals in mind. Our primary task is to explore how binary properties vary with environment, in particular to search for evidence of different binary frequencies among massive stars in clusters and associations and those in the field (especially runaway stars). A second goal is to compare the binary statistics in this angular range with those for close spectroscopic and wider separated systems in order to place constraints on the overall period distribution of massive binaries. Third, we identify individual systems of particular interest where the distant companion may influence our interpretation of the spectra or light curve of the primary target and may serve for future mass determination through measured orbital motion. We describe the observations and sample in Section 2, and then discuss the binary detection methods and results in Section 3. The issues surrounding companion frequency and period distribution are outlined in Sections 4 and 5, respectively, and we summarize our conclusions in Section 6.

2. FGS OBSERVATIONS

The FGS on board the *HST* acts as a single aperture shearing interferometer that forms interference fringes through a Koesters prism due to tilt differences in the incoming wavefront (Nelan et al. 2014). There are three FGS instruments on *HST* that are used for precise pointing of the telescope, and one of these, FGS1r, is designated for science applications. In the TRANS mode of operation, the FGS1r scans across the target in two orthogonal directions, and it produces an x and y coordinate fringe visibility curve (or "S-curve"). FGS observations of binary stars produce an S-curve that is the sum of fringe patterns for each component at a position that corresponds to the projection of the binary separation along the x and y vectors (Section 3).

The observations began as a SNAP program in Cycle 16 (GO-11212), and we selected targets all around the sky so that they could be easily scheduled into one-orbit slots between other programs. It was subsequently expanded into a Director's Discretionary program (GO-11901, 11943, 11944) around the time of the last servicing mission in order to optimize telescope usage when options with other instruments were very limited. Consequently, the observations were made over the period 2007–2009 in a large number of single-orbit pointings. All the observations were made with the ND 5 filter (brighter targets) or F583W filter (fainter targets) that record a broad range of the optical spectrum[10] ($\approx 4600-7000$ Å). Multiple scans were

recorded for each target with an angular step size of 1 mas, and the scans usually extended $\pm 1''0$ from the main target (or longer in some cases where a wider companion was known). Note that the FGS detectors record all the flux from sources within the field of view (FOV $\approx 5 \times 5$ arcsec^2), and although the detector response is uniform close to the target, the photometric response varies significantly for sources near the edge of the FOV. Special calibration is necessary to obtain reliable magnitude differences for companions near the periphery.

All the observations were processed with the FGS pipeline software (Nelan et al. 2014). First, the archived observations were extracted into individual scans using CALFGSA, which was also used to assess the data quality and to create a number of associated files that document the properties of the scans and observations. Then we used the routine PTRANS to gather the individual scans, coalign them, and spatially smooth the combined results. Finally, we applied a simple spline fit to rectify the distant parts of each summed scan to a zero average.

We selected our targets primarily from the Galactic O-Star Catalog[11] (Maíz-Apellániz et al. 2004, 2013), which we supplemented with other fainter targets from the catalog of Cruz-González et al. (1974) and with a selection of luminous blue variable (LBV) stars (van Genderen 2001). Two interlopers were accidentally included in the sample, the hot subdwarf CD-45°5058 = KS 292 (Rauch et al. 1991) and the K-giant BD-3°2178 (Pickles & Depagne 2010), which has been confused in the literature with the nearby hot subdwarf BD-3°2179. Both of these (apparently single) stars are excluded from the discussion in Sections 4 and 5. The targets are listed in order of increasing right ascension in Table 1, which provides the celestial coordinates, star name, the Johnson V magnitude, and $B - V$ color (Mermilliod & Mermilliod 1994). Column 5 gives the spectral classification of the brightest component from (in most cases) Sota et al. (2011, 2014); LBV classifications are from contemporaneous spectra described by Richardson et al. (2012). Columns 6–10 give information about the star's environment, runaway status, distance, spectroscopic binary status, and a recent spectroscopic reference, all gathered from a literature search for each object (see Section 4). Column 12 summarizes the number of companions detected in the FGS observations (Section 3), and the number of additional companions detected through spectroscopy or as wide visual binaries are given in columns 11 and 13, respectively (see Section 4). Column 14 lists other commonly used names for the targets and a code to identify the LBV (or candidate LBV) stars.

3. COMPANION STAR DETECTION

The detection of the signal of a stellar companion in the FGS scans depends primarily on the angular projected separation and magnitude difference. Each star in the FGS FOV produces a fringe pattern, and the observed scan will take the form

$$S(x)_{\mathrm{obs}} = \sum_{i=1}^{n} f_i \, S(x - x_i), \qquad (1)$$

where each of n stars contributes a flux fraction $f_i = \frac{F_i}{\sum F_j}$ and has a relative projected offset position x_i. The function $S(\triangle x)$ represents the apparent fringe pattern produced by a single


Table 1
Stellar Parameters

(α, δ) (J2000) (1)	Star Name (2)	V (mag) (3)	$B - V$ (mag) (4)	Spectral Class. (5)	C/A/F Category (6)	Runaway Status (7)	d (kpc) (8)	Spec. Status (9)	Spectroscopic Reference (10)	N (SB) (11)	N (FGS) (12)	N (WDS) (13)	Notes (14)
000603.39+634046.8	HD 108	7.39	0.17	O8 fpvar	Cas OB5	no	2.0	C	Nazé et al. (2001)	0	0	2	⋯
001743.06+512559.1	HD 1337	6.02	−0.05	O9.2 II	Field	yes	3.9	SB2OE	Stickland (1997)	1	0	3	AO Cas
014052.76+641023.1	HD 10125	8.22	0.31	O9.7 II	Field	no	2.7	SB1?	Williams et al. (2011)	1	1	1	⋯
022254.29+412847.7	HD 14633	7.46	−0.20	ON8.5V	Field	yes	2.2	SB1O	McSwain et al. (2007)	1	1	1	⋯
022759.81+523257.6	HD 15137	7.87	0.03	O9.5 II-IIIn	Field	yes	2.7	SB1O	McSwain et al. (2007)	1	0	0	⋯
023249.42+612242.1	HD 15570	8.11	0.69	O4 If	IC 1805	no	1.9	C	Hillwig et al. (2006)	0	0	0	⋯
024044.94+611656.1	HD 16429	7.67	0.62	O9 II-III(n)Nwk	Cas OB6	no	1.8	SB3O	McSwain (2003)	1	1	3	⋯
024252.03+565416.5	HD 16691	8.70	0.48	O4 If	Per OB1	no	1.8	C	De Becker et al. (2009)	1	0	0	⋯
025107.97+602503.9	HD 17505	7.07	0.40	O6.5 IIIn(f)	IC 1848	no	1.8	SB3O	Hillwig et al. (2006)	2	1	9	⋯
025114.46+602309.8	HD 17520A	8.26	0.32	O8 Vz	IC 1848	no	1.8	SB2?	Hillwig et al. (2006)	1	1	13	⋯

Note. 1 = LBV or LBV candidate; 2 = FGS data from Nelan et al. (2004, 2010); 3 = FGS data from Caballero-Nieves et al. (2014).

(This table is available in its entirety in machine-readable and Virtual Observatory (VO) forms.)
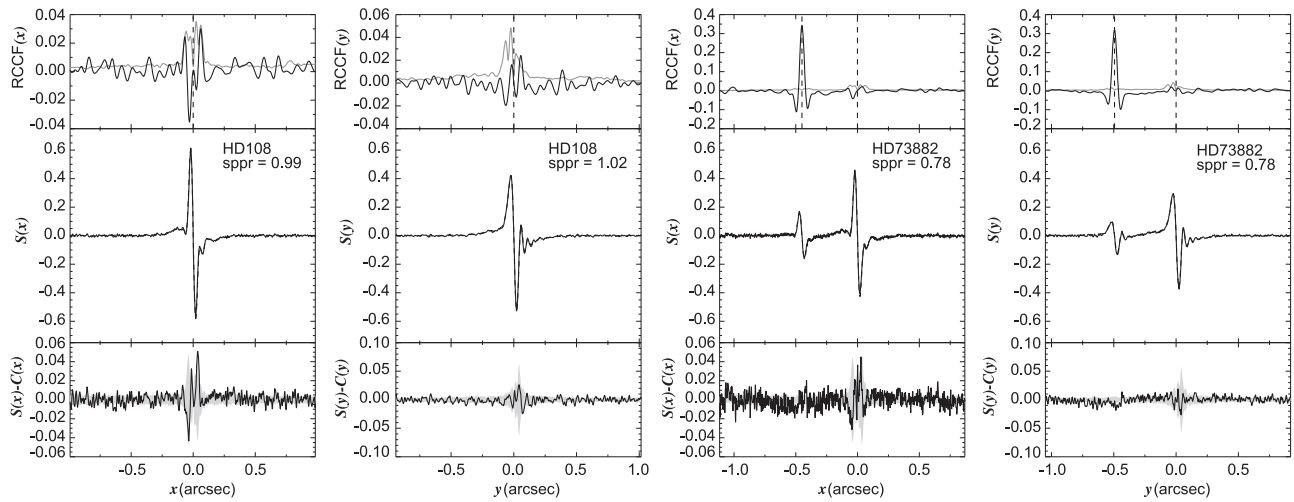
Figure 1. (A) FGS scans and binary detection tests for the single star target 000603.39+634046.8 = HD 108 obtained on BY 2008.5566. (B) The FGS scans and binary detection tests for the binary star target 083909.53−402509.3 = HD 73882 obtained on BY 2008.4061.

The complete figure set (251 images) is available.

Table 2
Resolved Companions

(α, δ) (J2000) (1)	Star Name (2)	Discovery Designation (3)	Date (BY) (4)	FGS Filter (5)	θ (deg) (6)	ρ (arcsec) (7)	$\triangle m$ (mag) (8)	Figure 1.n (9)	Notes (10)
014052.76+641023.1	HD 10125	HDS 221 AB	2008.0775	F583W	231.14 ± 0.10	0.7216 ± 0.0007	3.509 ± 0.085	3	⋯
022254.29+412847.7	HD 14633	FGS 1 Aa,Ab	2007.8425	F5ND	352.31 ± 32.32	>0.0197 ± 0.0111	1.643 ± 1.083	4	2
024044.94+611656.1	HD 16429	CHR 208 Aa,Ab	2007.6831	F5ND	91.16 ± 0.16	0.2849 ± 0.0008	2.150 ± 0.040	7	⋯
025107.97+602503.9	HD 17505	STF 306 AB	2008.5621	F5ND	⋯	>0.2115 ± 0.0007	1.918 ± 0.054	9	1,5
025114.46+602309.8	HD 17520A	BU 1316 AB	2008.2139	F583W	298.83 ± 0.08	0.3174 ± 0.0008	0.553 ± 0.020	10	⋯

Note. 1 = see the Appendix; 2 = resolved on the x-axis, unresolved on the y-axis, so the position angle and separation are estimated assuming $\triangle y = 0$; 3 = resolved on the y-axis, unresolved on the x-axis, so the position angle and separation are estimated assuming $\triangle x = 0$; 4 = resolved on the x-axis, off scan on the y-axis, so no position angle is listed and only a lower limit on the separation is given; 5 = resolved on the y-axis, off scan on the x-axis, so no position angle is listed and only a lower limit on the separation is given; 6 = reassignment of bright star designation for consistency with WDS.

(This table is available in its entirety in machine-readable and Virtual Observatory (VO) forms.)

unresolved star. We show in the figure set the full collection of 251 merged scans of our targets associated with Figure 1, and the central two panels of these figures show the final scans along the orthogonal x and y axes. A single star (see, e.g., HD 108, Figure 1(A)) shows a simple fringe oscillation pattern, while a fully resolved binary star (see, e.g., HD 73882, Figure 1(B)) shows two clearly separated fringe patterns. In general, the relatively bright and widely separated companions are immediately detected upon inspection, but detection is more challenging with fainter companions or those cases of close companions where the fringe patterns largely overlap. Our detection scheme relies upon a comparison of the observed scans with those for a set of single stars that act as calibrator scans. We first apply a set of detection tests developed by Caballero-Nieves et al. (2014) and, if a resolved component is found, then we make a detailed fit of the observed scan with a selection of calibrator scans. Below we review the testing criteria and fitting procedure, and our results are summarized in Table 2 for resolved systems, Table 3 for partially resolved systems, and Table 4 for apparently single, unresolved systems.

The detailed form of the fringe pattern $S(\triangle x)$ depends upon the color of the star and filter used (Horch et al. 2006) as well as the time of observation relative to that of a servicing mission

or other adjustments of the instrument. We selected the calibrators from a set of scans that appeared to be those of single stars from our program (see Table 4 below) and of red, low-mass stars observed in programs GO-11943 and 11944. These scans were subsequently checked for binary interlopers with the tests described below before establishing final lists of calibrator scans. The scans were arranged into four categories based on filter (FND 5 or F583W) and time of observation (before or after the final servicing mission on BY 2009.06), and they were ordered according to $B − V$ color. In most cases, we relied upon all the available calibrators with colors within ±0.5 mag of the target's $B − V$ color (usually numbering between 6 and 50 cases).

The first clues about the presence of a companion come from a visual inspection of the scans for multiple fringe patterns and from a measurement of the fringe amplitude dilution caused by the flux of the other star(s) (see Equation (1)). The latter is measured by the S-curve peak-to-peak amplitude ratio (given as "sppr" in the central panels of Figure 1), which is the mean of the ratio of observed to calibrator full amplitude among the set of selected calibrators. A value of sppr <0.92 is often an indication of the presence of another flux source in the FGS FOV (Caballero-Nieves et al. 2014).

Table 3
Partially Resolved Companions

(α, δ) (J2000) (1)	Star Name (2)	Discovery Designation (3)	Date (BY) (4)	FGS Filter (5)	$^a\theta_1$ (deg) (6)	$^a\theta_2$ (deg) (7)	ρ_{min} (arcsec) (8)	Figure $1.n$ (9)	Notes (10)
053516.47−052322.9	HD 37022C	WGT 1 Ca,Cb	2007.9029	F5ND	247 ± 19	35 ± 19	0.0151 ± 0.0025	34	⋯
075557.13−283218.0	HD 65087	FGS 33 AB	2008.8784	F583W	221 ± 14	16 ± 14	0.0168 ± 0.0019	117	⋯
104505.85−594006.4	HDE 303308	NEL 5 Ha,Hb	2008.5511	F583W	100 ± 19	174 ± 19	0.0096 ± 0.0025	172	1
104505.85−594006.4	HDE 303308	NEL 5 Ha,Hb	2008.8819	F583W	195 ± 15	155 ± 15	0.0114 ± 0.0019	173	1
110840.06−604251.7	V432 Car	FGS 34 AB	2008.9337	F583W	209 ± 8	349 ± 8	0.0118 ± 0.0006	182	⋯
110840.06−604251.7	V432 Car	FGS 34 AB	2008.9337	F583W	240 ± 10	318 ± 10	0.0075 ± 0.0014	183	⋯
174159.03−333013.7	HD 160529	FGS 35 AB	2009.2643	F5ND	191 ± 17	11 ± 17	0.0084 ± 0.0037	208	⋯
174159.03−333013.7	HD 160529	FGS 35 AB	2009.2643	F5ND	219 ± 5	342 ± 5	0.0131 ± 0.0009	209	⋯
180352.44−242138.6	HD 164794	FGS 36 AB	2008.1920	F5ND	246 ± 13	292 ± 13	0.0185 ± 0.0019	213	⋯
203034.97+441854.9	HD 195592	FGS 37 AB	2008.5326	F5ND	105 ± 59	285 ± 59	0.0108 ± 0.0011	239	⋯

Note. 1 = see the Appendix.

Table 4
Unresolved Targets

(α, δ) (J2000) (1)	Star Name (2)	Date (BY) (3)	FGS Filter (4)	Figure $1.n$ (5)	Notes (6)
000603.39 + 634046.8	HD 108	2008.5566	F5ND	1	⋯
001743.06 + 512559.1	HD 1337	2008.7090	F5ND	2	⋯
022759.81 + 523257.6	HD 15137	2007.6777	F5ND	5	⋯
023249.42 + 612242.1	HD 15570	2007.6478	F583W	6	⋯
024252.03 + 565416.5	HD 16691	2007.5274	F583W	8	⋯

Note. 1 = see the Appendix.

(This table is available in its entirety in machine-readable and Virtual Observatory (VO) forms.)

We tested for the presence of resolved companions using a cross-correlation function (CCF) method developed by Caballero-Nieves et al. (2014). This is an iterative scheme that compares the CCF of a target with a calibrator scan to the CCF of the calibrator with itself. The first step is to align and rescale the calibrator CCF with the main peak in the target CCF, and then this rescaled calibrator CCF is subtracted to search for residual peaks in the target CCF from companions. The results of this first step (denoted RCCF for "residuals from the CCF subtraction") are shown in the top two panels of Figure 1. A vertical dashed line at the origin shows the position where the primary signal was removed. Then, we sequentially identify any remaining CCF peaks that attain a strength $>4\sigma(\text{CCF})$, where $\sigma(\text{CCF})$ is the standard deviation at that scan position among the collection of calibrator scan CCFs (shown as the light gray line in the upper panels of Figure 1). These peaks are also indicated by vertical dashed lines in Figure 1. Then, we use the scaling and offset parameters for each identified component to make a model composite scan, which is shown as a dashed line in the central panels (often hidden within the line thickness of the observed scan plot). Finally, the difference between the observed and model scans is shown on an expanded amplitude scale in the lower panels of Figure 1, where the $\pm\sigma(\text{CCF})$ region is indicated by light gray shading.

Note that all the CCF results shown in Figure 1 refer to a mean CCF derived from the CCFs of the target with each of the selected calibrator scans. Most of our targets are relatively bright and the merged scans have good signal-to-noise ratio (S/N) properties, so the main source of uncertainty in binary detection is related to how well the calibrator scans match the target scan. Consequently, the detection criterion for a CCF peak is based on its strength relative to the scatter we find among the calibrator scans. Simulation tests made by Caballero-Nieves (2012) indicate that our $>4\sigma(\text{CCF})$ criterion will result in no more than a single accidental detection in a sample as large as ours. Indeed, there are potentially other plausible detection cases that can be made by inspection of the CCF plots in Figure 1, but for the purposes of this paper, we generally include only those that meet this stringent requirement in order to avoid false detections.

The CCF method yields ambiguous results for very close companions (with projected separations generally less than 20 mas) because in the first iteration the calibrator CCF will be matched to a position between the components where the composite CCF peaks. In such a situation the residual CCF will show two comparable peaks around the origin. Hence we require a second test to deal with close binaries that create blended fringe patterns. Caballero-Nieves et al. (2014) showed that in such blended cases the difference between the observed

and calibrator scans will have a functional shape proportional to the second derivative of the calibrator scan,

$$
\begin{aligned}
S(x)_{\mathrm{bin}} - S(x)_{\mathrm{cal}} &= \frac{1}{1+r} S\left(-\left(\frac{r}{1+r}\right)\Delta x\right) \\
&\quad + \frac{r}{1+r} S\left(+\left(\frac{1}{1+r}\right)\Delta x\right) - S(x) \\
&= \frac{1}{2}\frac{r}{(1+r)^2}(\Delta x)^2 S''(x) \equiv a S''(x), \quad (2)
\end{aligned}
$$

where Δx is the projected separation and $r = F_2/F_1$ is the flux ratio. This relation shows that the single parameter a that can be derived from the blend is a function of both r and $|\Delta x|$, so that these parameters cannot be determined independently. However, the relation also demonstrates that close binaries can be detected by searching for those cases where the amplitude of the second derivative coefficient a is large and positively valued. We applied this second derivative test for detection by requiring $a > 4\sigma(a)$, where a and $\sigma(a)$ are the mean and standard deviation of the fits of Equation (2) from the set of selected calibrator scans. Those cases that met this criterion are shown with a thick gray line portraying the fit in the lower panels of Figure 1 (see, e.g., HD 65087, Figure 1.117).

Once we had identified those resolved components with the CCF method, we then made a non-linear, least squares fit of the scans using the Levenberg–Marquardt algorithm with the IDL function *mpfitfun* (Markwardt 2009). We did not make fits for the close blended scans because of the inherent ambiguity in the parameters in such cases (see Equation (2)). The binary or triple-star fit was made of the positions and amplitudes of the fringe patterns for each component using a model of the form of Equation (1) but with independent parameters for the amplitude of each component. Starting values for each parameter were taken from the CCF results. The fits were made with each selected calibrator, and the final adopted values and uncertainties were estimated from the mean and standard deviation of the fitting parameters from the calibrator set.

We found that it was preferable to have independent amplitude scaling parameters for each component (rather than coefficients referenced to the flux of the primary as in Equation (1)) in order to deal effectively with the general scaling mismatch between the target and calibrator scans. The magnitude differences were then obtained as $-2.5 \log F_i/F_1$ for each component. In order to check our results, we compare in Figure 2 the derived magnitude differences (mean of x- and y-axis fits) with those obtained by *Hipparcos* (Perryman & ESA 1997) for some of the mutually detected wide binaries. The excellent agreement indicates that our magnitude estimates and their uncertainties are apparently reliable and free of systematic problems.

There are generally four possible outcomes for binary detection along each axis: (1) the fringe appearance is consistent with that of a single star, (2) the second derivative test indicates a blended component, (3) the fringes of a companion are resolved by the CCF test, or (4) a companion exists beyond the scan range but within the FGS FOV and causes a dilution of the fringe amplitude of the target (see Equation (1)). If a system is triple, then the same set of outcomes is possible for the third component (all dependent upon the orientation of the component in the sky relative to the scan axes). We attempted to decide upon these outcomes based upon an inter-comparison of the test results between axes and

the parameters of those known binary systems. The Appendix provides notes about those cases where the outcomes were ambiguous or problematical.

The results for systems that were resolved along at least one axis are collected in Table 2. The entries are listed in order of increasing right ascension and by date of observation where multiple observations were made. Columns 1 and 2 give the coordinates and name (same as in Table 1), and column 3 gives the discovery designation from the Washington Double Star (WDS) Catalog (Mason et al. 2001).[12] If the FGS observation is the first detection, then "FGS" is listed along with a component designation made following the nomenclature used in the WDS (Hartkopf & Mason 2004). Columns 4 and 5 give the date and filter for the observation. Columns 6–8 give the position angle θ, separation ρ, and magnitude difference Δm determined by our non-linear, least squares fits of the scans. In most cases the component is resolved in both axes. Then the position angle is determined from the projected axial separations and the telescope orientation on the sky (from the PA_APER keyword in the observation header file), the separation is the square root of the sum of the squares of the projected axial separations, and the magnitude difference is the error weighted average of the x and y values. In other cases, the component is resolved on only one axis, but has a significant second derivative coefficient a for the other axis. Then the absolute value of the close separation $|\Delta x|$ is derived using the flux ratio r from the resolved axis result and the relation between a, r, and $|\Delta x|$ from Equation (2). This yields a reliable value for ρ, but there are two possible θ angles that correspond to the choice of $\pm|\Delta x|$. We list in Table 2 the θ estimate for $+|\Delta x|$ and the Appendix notes give the other possible θ value. There are several cases where the companion is probably beyond the scan range along one axis, and for these there is no θ estimate and only a lower limit for ρ. Column 9 gives the number of the Figure 1 plot that corresponds to the observation, and column 10 provides codes for notes about the specific system.

Table 3 lists those cases where the second derivative test indicated the presence of a blended component along at least one axis (and the target is not included in Table 2). Table 3 has the same format as Table 2, except for columns 6–8 that are used differently. The second derivative coefficient a depends on both flux ratio and separation (see Equation (2)), and we can set a minimum separation for a flux ratio $r = 1$,

$$
\rho_{\mathrm{min}} = \sqrt{8}\,\sqrt{a_x + a_y}, \quad (3)
$$

where a_x and a_y are the positively valued, second derivative coefficients measured for the x and y scans, respectively. This lower limit is given in column 8 of Table 3. If the flux ratio r eventually becomes known, then the actual separation will be given by

$$
\rho = \rho_{\mathrm{min}}\frac{1+r}{2\sqrt{r}}. \quad (4)
$$

There is a four-fold ambiguity in the derived position angle θ depending on the signs of Δx and Δy. Columns 6 and 7 give $^a\theta_1$ which is the ambiguous position angle for $(+|\Delta x|, +|\Delta y|)$ and $^a\theta_2$ which is the ambiguous position angle for $(+|\Delta x|, -|\Delta y|)$; add 180° to each of these to arrive at the

---

[12] http://ad.usno.navy.mil/USNO/astrometry/optical-IR-prod/wds/WDS
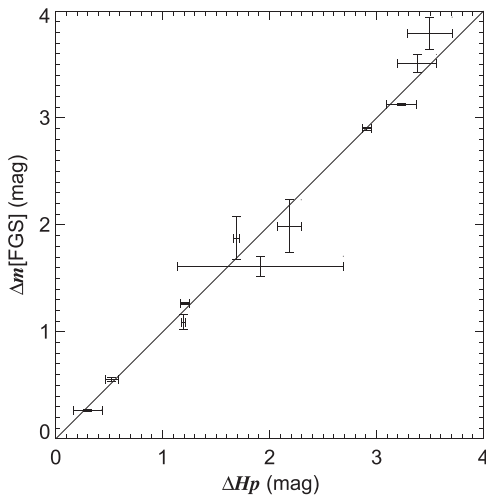
Figure 2. Comparison of magnitude differences from *Hipparcos* and FGS for pairs in common. The estimates agree within uncertainties with the expected one-to-one relationship (shown as a solid line of slope unity).

remaining two possibilities. We can check on the validity of these estimates for the second derivative detection of a close companion of HD 37022C = θ^1 Ori C that is a binary with an orbit derived from long baseline interferometry (Kraus et al. 2009). Kraus et al. (2009) report a VLTI measurement at about the same time as the *HST* FGS observation with $\rho = 19.1$ mas and $\theta = 241°$. If we adopt their optical flux ratio $r = 0.30$, then Equation (4) and ρ_{min} yield estimates of $\rho = (17.9 \pm 3.0)$ mas and $\theta = (247 \pm 19)°$, in agreement with the contemporaneous VLTI measurement.

Table 4 lists the remaining systems for which we find no evidence of a companion. The format of Table 4 consists of the same first four and last two columns of Table 2. Altogether, of our sample of 226 stars, we resolved 52 binary and 6 triple systems (Table 2), partially resolved 7 binaries (Table 3), leaving 161 stars unresolved (Table 4). Only 29 of the systems were known prior to this FGS survey.

We show in Figure 3 the total separations and magnitude differences for all the components that we detected. The partially resolved systems are plotted assuming that the components have the same flux ($r = 1$). The solid line connecting diamond-shaped symbols shows the expected faint limit for companion detection by the CCF method, and the dotted line illustrates the expected limit for detection of close companions by the second derivative test (all for similar FGS scans from Caballero-Nieves et al. 2014). Our detections fall within the expected range for the most part, reaching as faint as $\triangle m = 5$ for widely separated binaries (but less for closer binaries). The smallest separations we can detect are about 10 mas (Table 3). For example, while we did detect the close binary HD 37022C = θ^1 Ori C ($\rho = 19.1$ mas; Figure 1.34), we failed to resolve the relatively bright companion of HD 150136 (Figure 1.196) with a separation of 7 mas (Sana et al. 2013a; Sanchez-Bermudez 2013).

4. COMPANION FREQUENCY

We found that 65 of 224 targets (omitting the subdwarf CD-45°5058 = KS 292 and the K-giant star BD-3°2178) or 29% of the sample have a visual companion in the angular range from $0''01$ to $1''0$. This detection rate compares well with earlier

surveys of massive stars in the Carina Association (22%; Nelan et al. 2004, 2010) and in Cyg OB2 (22%; Caballero-Nieves et al. 2014). We find 6 of the 13 LBV or candidate LBV stars to have companions, but 4 of these are located in the LMC where source crowding is an issue, so we do not consider this high binary fraction to be unusual. However, in order to study the total multiplicity fraction, we must also consider what is known about closer binaries (detected as spectroscopic binaries) and wider binaries (detected by speckle interferometry, adaptive optics, and other astrometric methods). We have collected information on the binary companions of our sample through a literature review of the spectroscopic properties and a search through the WDS catalog for wider pairs. Furthermore, we have supplemented our sample of 224 stars with 81 others from the prior FGS surveys: 23 stars in the Carina association (Nelan et al. 2004, 2010; omitting HDE 303308 which is already part of our main survey) and 58 stars from the Cyg OB2 association (Caballero-Nieves et al. 2014). The information on these additional 81 stars is gathered at the bottom of Table 1 for convenience. Table 1, column 9 lists a code describing the spectroscopic status and column 10 gives a reference for the literature source. Spectroscopic binaries are identified with the code "SB" that is usually followed by the number of spectral components observed (one for a single-lined binary, two for a double-lined binary, and higher if additional components are known). The code may include a suffix of "O" for systems with orbital determinations, "E" for eclipsing or ellipsoidal systems, and "?" for suspected systems (for example, for systems with a large radial velocity range but no orbit or those where double lines are reported). A code of "C" indicates a star with apparent constant radial velocity. Many of the targets are assigned a code of "U" for unknown status in cases where there are only a few or no radial velocity measurements. The total number of probable spectroscopic companions (not including those detected in the FGS survey) is listed in column 11 of Table 1. Columns 12 and 13 give the numbers of visual companions found in our survey and from inspection of the WDS, respectively.

We are also interested in the binary properties as a function of environment because stars ejected from their natal clusters may preferentially be single stars. Column 6 of Table 1 lists the name of the cluster or association of membership or the entry "Field" if no membership is known. Most of these assignments come from earlier work by Humphreys (1978), Moffat et al. (1979), Garmany et al. (1982), and the cluster database WEBDA.[13] We note that several of these "clusters" are in fact groups of only several luminous stars, but nevertheless, their existence shows that the target still resides among the stars where it was born. de Wit et al. (2005) have shown that some so-called field stars are the brightest members of clusters with a host of fainter stars (e.g., HD 52533, HD 195592), and we suspect that many of the targets assigned to the field category in Table 1 may turn out to be members of unrecognized clusters. The runaway stars in the sample (Mason et al. 2009) are indicated by an entry of "yes" in column 7 of Table 1.

We caution that some of the wider, resolved companions may be field stars along the line of sight. Furthermore, some of the targets reside in rich star clusters, and their companions may be cluster members that are not necessarily orbiting the

---

[13] http://www.univie.ac.at/webda/webda.html
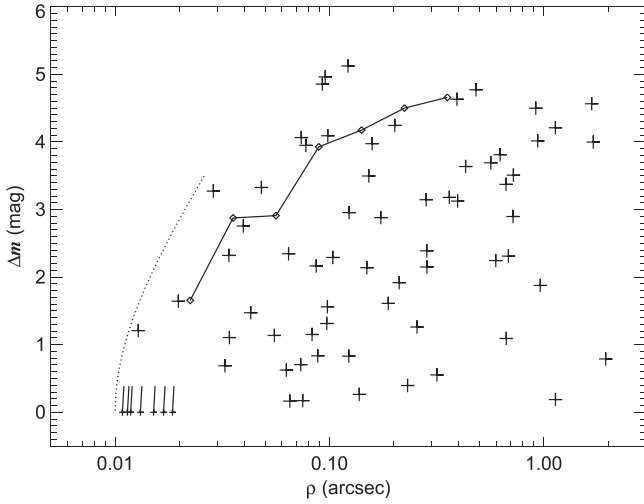
Figure 3. Fitted projected separation ρ and magnitude difference $\triangle m$ for the resolved pairs (large plus signs) and the partially resolved pairs (small plus signs with line segments showing the displacement from $\triangle m = 0.0$ to 0.4, i.e., for $F_2/F_1 = 1.0$ to 0.7). The diamonds connected by a solid line represent the expected faint limits for detection by the cross correlation method and the dotted line shows the corresponding faint limit for detection by the second derivative test (Caballero-Nieves et al. 2014).

primary target. The probability of such a chance alignment may be estimated from the nearby surface density of stars with a magnitude less than that of the companion, $\Sigma(V < V_c)$. Correia et al. (2006) show that the probability of finding a field star at a separation ρ from the target is given by

$$p(\Sigma, \rho) = 1 - e^{-\pi\Sigma\rho^2}. \qquad (5)$$

We estimated Σ in practice by collecting stellar F-magnitudes (covering the 579–642 nm range) in the region within a radius of $15'$ from the target that we extracted from the UCAC4 catalog (Zacharias et al. 2013). We then formed cumulative distribution functions with magnitude for each set and made a linear fit of the logarithm of cumulative star counts with magnitude (Lafrenière et al. 2014). We used this fit to estimate Σ for the magnitude of a given companion star, and then we estimated the probability of chance alignment for the companion's projected separation ρ. Companions with a probability $p < 0.01$ are good candidates for physically related objects.

The companions detected in the FGS survey have small projected separations and are generally bright, so the probability of a chance alignment is much smaller than the $p = 0.01$ criterion. However, the situation is different for some of the more widely separated companions in the WDS sample. For example, there are seven companions listed in the WDS for HD 190918, but only four of these meet the probability criterion. This star is a member of the open cluster NGC 6871, so it is possible that the remaining three companions are cluster members. Long-term proper motion investigations will be required to determine which of these companions are actually gravitationally bound to HD 190918.

Additional factors should be considered in assessing the status of the companions listed in the WDS. For example, the runaway star HD 34078 = AE Aur is listed with three companions in the WDS. This is a surprising result because this star was probably ejected from the Ori OB1 association through an encounter between binary stars (Gualandris

Table 5
Frequency of Multiple Systems and Companion Frequency

Group (Number)	Cluster/Association (214)	Field (58)	Runaway (29)
A. FGS Visual Binaries			
n(FGS)	67	9	2
MF(FGS)	0.31 ± 0.03	0.16 ± 0.05	0.07 ± 0.05
CF(FGS)	0.34 ± 0.04	0.17 ± 0.05	0.07 ± 0.05
B. WDS Visual Binaries			
n(WDS)	61	10	10
MF(WDS)	0.29 ± 0.03	0.17 ± 0.05	0.34 ± 0.09
CF(WDS)	0.84 ± 0.14	0.22 ± 0.07	0.52 ± 0.16
C. Spectroscopic Binaries			
n(SBO+E)	68	5	5
n(SB?)	28	14	3
n(C)	65	14	21
n(U)	53	25	0
MF(SBO+E)	0.42 ± 0.04	0.15 ± 0.06	0.17 ± 0.07
MF(SBO+E+?)	0.60 ± 0.04	0.58 ± 0.08	0.28 ± 0.08
CF(SBO+E)	0.51 ± 0.05	0.15 ± 0.06	0.17 ± 0.07
CF(SBO+E+?)	0.68 ± 0.05	0.58 ± 0.09	0.28 ± 0.08
D. Any Companion			
MF(min)	0.51 ± 0.03	0.21 ± 0.05	0.21 ± 0.07
MF(max)	0.69 ± 0.03	0.50 ± 0.06	0.48 ± 0.09
CF(min)	0.70 ± 0.06	0.26 ± 0.07	0.24 ± 0.09
CF(max)	1.67 ± 0.17	0.72 ± 0.11	0.86 ± 0.20

et al. 2004), and the star is expected to be single at present. A closer examination of the notes in the WDS indicates that the Aa, Ab companion is an artifact of AO imaging and that the AB companion is "very doubtful." Furthermore, according to UCAC4, the AC companion is probably 3.5 mag fainter than the magnitude listed in the WDS, so that its probability of chance alignment is above the adopted criterion. The tentative conclusion is that HD 34078 has no physically related companions, consistent with expectations. However, for the purposes of this work, we decided to retain all the companions listed in the WDS, pending the further research that will be required to settle their true nature. Thus, we caution that the companion numbers presented here from the WDS sample must be regarded as probable overestimates of the actual numbers of bound companions.

Table 5 summarizes the numbers of companions according to their environmental parameter: cluster/association, field, or runaway groups. We removed the four targets in the LMC from the total sample ($n = 224 + 81 - 4 = 301$) because of crowding issues related to the large distance of the LMC. The companion numbers are first presented in section A for the resolved binaries in the FGS sample. The number n(FGS) gives the number of targets with one or more detected companions in each environmental group. The next row gives the corresponding frequency of multiple systems (MF = number with any companion divided by the total number). The uncertainty estimates are based upon the binomial statistical approach of Cameron (2011) for a confidence interval of $c = 0.683$ (equivalent to 1σ), and they represent the average of the almost equal lower and upper confidence limits. The third row reports

the companion frequency (CF = number of companions divided by the number of targets). The uncertainties in this case were estimated by a bootstrap method of random sampling of the data in the subsets (see Raghavan et al. 2010). The three rows in section B of Table 5 give the same values for the WDS sample. The estimates of MF are similar for the two samples and the cluster/association and field stars, but the MF estimate for the runaway stars and the CF estimates are all larger for the WDS sample. We suggest that this is due to overestimates of companion numbers in the WDS.

Section C of Table 5 lists the same n, MF, and CF values for the spectroscopic binaries in this sample. The number n (SBO+E) counts the number of targets with known orbital periods, i.e., those with spectroscopic orbits and/or eclipsing light curves. The next three rows list the corresponding numbers for possible spectroscopic binaries (with a status listing of "SB1?" or "SB2?" in Table 1), constant velocity stars, and stars with unknown spectroscopic binary properties, respectively. Stars in the latter group were omitted in the calculation of MF and CF for the spectroscopic binaries. The next four rows give the MF and CF estimates based upon two samples of the spectroscopic binaries, those with known period (SBO+E) and those known and suspected binaries (SBO+E+?).

Section D of Table 5 gives the combined MF and CF estimates for two counting schemes. The first combines the numbers of spectroscopic binaries with known period plus the numbers of FGS binaries. In this case we ignore any suspected spectroscopic binaries and all the WDS companions, so these statistics are noted as $MF(\min)$ and $CF(\min)$ because they represent reliable minimum fractions. The second counting scheme sums all the known and suspected spectroscopic binaries, FGS companions, and WDS companions. These are representative of the observed maximum fractions, because they include some spectroscopic targets that may be velocity variable for reasons other than a binary companion and they include some unrelated companions from the WDS catalog.

The high frequency of multiple systems among the SB category is similar to that found in recent spectroscopic surveys (Chini et al. 2012; Sana et al. 2012, 2013b; Sota et al. 2014), and our results confirm the trend that the ejected stars (runaway and some field stars) have a lower frequency of multiple systems than stars still in their natal clusters. This trend is also seen among the FGS visual binaries, but it is probably absent for the WDS sample because the bound companion numbers are overestimated for our WDS sample (recall the case of the runaway star AE Aur discussed previously). The relatively high frequency of multiple systems among the resolved binaries is also striking, and this verifies the importance of the more distant companions to the total numbers of companions (Mason et al. 1998, 2009; Peter et al. 2012). The companion frequency is also very high among the cluster/association stars, reaching a value between 0.7 and 1.7 companions per target after combining the SB, FGS, and WDS samples.

The numbers presented in Table 5 represent the properties of observed companions, and transforming these into the total numbers of multiple systems requires a careful consideration of observational selection effects and assumptions about the period and mass ratio distributions (Kiminki & Kobulnicky 2012; Sana et al. 2013b). For example, the FGS survey is limited to companions brighter than $\triangle m = 5$, which corresponds approximately to $M_2/M_1 > 0.1$, so we miss

companions with a mass below a few solar masses. Such faint companions may be detected with AO imaging over a limited angular separation range (Turner et al. 2008), but such AO observations are incomplete for our sample. Single high-resolution measurements may also miss those systems that are close to a small separation conjunction phase at the time of observation. The spectroscopic binary numbers are based on observations with very diverse spectral resolution, wavelength coverage, and temporal cadence properties, and we suspect that many more binaries will be detected and/or verified in ongoing radial velocity investigations. Furthermore, the diversity of mass, age, and orbital periods in our sample may mix populations with differing binary properties (Kaczmarek et al. 2011). The binary statistics in Table 5 should therefore be regarded as the result of a convolution of the actual distributions with the observational selection effects that limit detections.

5. ORBITAL PERIOD DISTRIBUTION

We collected from the literature orbital periods for 83 of the SBO or SBE binary systems listed in Table 1. The visual binaries have much longer periods that are only beginning to be sampled, and there are published periods for only five visual binaries in our sample (HD 37022, Kraus et al. 2009; HD 25639, Gorda et al. 2007; HD 37468, Turner et al. 2008; HD 47839, Cvetković et al. 2010; HD 193322, ten Brummelaar et al. 2011). However, we may obtain an approximate orbital period for the visual binaries by considering their angular separation, distance, and probable mass. The angular separation in the sky depends on orbital orientation and phase, and for circular orbits, we expect that the projected separation generally underestimates the actual semimajor axis. On the other hand, many long-period binaries have orbits with a large eccentricity, so that we observe them most of the time with a separation $(1 + e)\times$ larger than the semimajor axis. Brandeker et al. (2006) made Monte-Carlo simulations of the ratio of projected separation to semimajor axis for an ensemble of binaries with a commonly adopted eccentricity distribution $f(e) = 2e$, and they found that this ratio has a value of 1.0 ± 0.7, where the uncertainty represents the HWHM of the distribution (see their Figure 9). Consequently, we estimated the semimajor axis a for the visual binaries by $a \approx \rho d$, where a is measured in AU, ρ in arcseconds, and d in parsecs. Column 8 of Table 1 lists the adopted distances for the targets, which were taken from WEBDA for cluster members and from Mel'Nik & Dambis (2009) for association stars. Distances for the field stars were generally collected from spectroscopic parallaxes given by Garmany et al. (1980) or Gudennavar et al. (2012). If no distance estimate was found, then we calculated the spectroscopic parallax ourselves using the magnitude, colors, and spectral classifications in Table 1 with intrinsic colors from Wegner (1994), a ratio of total-to-selective extinction of $R = 3.1$, and absolute magnitudes from Balona & Crampton (1974) and Martins et al. (2005). We then estimated the orbital period P using Kepler's third law and mass estimates for the primary from the spectral classification —mass calibration of Martins et al. (2005; their Tables 4–6). Note that we have ignored the need to adjust the period upward because the spectroscopic parallaxes probably underestimate the true distance (binaries are brighter than the primary alone), and likewise ignored a downward period adjustment because the mass estimate is low (binaries are more massive than the

single primary). However, these changes are minor compared to the uncertainties inherent in our assumed equivalence of a and ρ. Our final tally of orbital periods for visual binaries in our sample amounts to 89 estimates for companions from the FGS detections plus 207 others for companions from the WDS catalog.

Our goal in this Section is to determine the frequency of multiple systems MF as function of the binary orbital period. This requires a determination of the number of targets in the sample for which our methods would probably find a binary over a given period range. Consequently, we need to consider the period range sensitivity for each method of binary detection. A fortunate spectroscopic observer may discover a binary in a single measurement of a double-lined system, but the determination of an orbital period for a spectroscopic binary generally requires a significant effort of repeated observations. Thus, the exploration space to determine a binary period grows with the number of observations and the duration between the first and last spectroscopic observations. We extracted this observational duration from the papers cited in Table 1 for each of the targets with a spectroscopic status different from "U" (unknown), and then we estimated the period detection range for each target as one day (smallest contact binary) to the full duration of observations. We then constructed a logarithmic period grid using time in years and a bin size of 1 dex, and we determined the number of targets in each period bin where the spectroscopic duration is sufficient to measure at least one binary orbital period. This summation included cases where only a fraction of the log P bin range was covered by adding the ratio of the covered range to the full 1 dex bin size. Then the multiplicity fraction was calculated as the ratio of number with measured periods to the summed number of targets for which detection was possible within each log P bin. Note that our simple characterization of the period detection range fails to represent the true complexity of the time series associated with the spectroscopic observations. For example, a series of nightly observations made over one week plus a single observation made one month later would be taken at face value as suitable to detect periods up to one month, when, in fact, such a series is most sensitive to periods of a week or less. Thus, by using only the full duration of the observing sequence, we probably overestimate the detection efficiency at longer periods, and this may lead to a modest underestimate of $MF(\log P)$ at the longer orbital periods associated with the spectroscopic observations.

We used a similar approach to find $MF(\log P)$ for the visual binaries detected in the FGS survey and listed in the WDS catalog. The period range of detectability for these cases depends on the projected separation, distance, and stellar masses, and we used the distances from Table 1 and masses from calibrations based upon spectral classification to determine P from projected angular separation (in the same way as we did for the detected binaries). The FGS scans are sensitive to binaries in the $0\rlap{.}''01$–$1\rlap{.}''0$ range, while the WDS appears to list systems over a broader range of $\approx 0\rlap{.}''1$ to $\approx 100''$. We adopted these angular ranges in setting the period range for binary detection for each target in our sample, and then we estimated the summed target number and multiplicity fraction in each log P bin in the same way as for the spectroscopic sample. Note that we took care not to double count those systems detected in the FGS survey that also appear in the WDS catalog.

We show our resulting $MF(\log P)$ relation as a set of histograms in Figure 4. The detected multiplicity fractions are shown individually for the SB, FGS, and WDS sets, and then the sum of these is shown as the final histogram (representing the total found from all methods). This summed distribution appears to be approximately flat, but we need to bear in mind a number of selection effects that may influence the appearance of the distribution. The low log P part of the distribution that is estimated from spectroscopic data is probably systematically low, because inclusion in the plot requires a significant observational effort, and we expect that a large fraction of the systems with a spectroscopic status of "SB1?" and "SB2?" in Table 1 will indeed turn out to be real short-period binaries. Furthermore, it is likely that observers may tend to favor short-period over long-period binaries, because of the extended labor required to determine periods for the long-period systems. On the other hand, it is relatively simple to estimate an approximate period for a visual binary from a single high angular resolution observation, and such observations are sensitive to relatively faint and lower mass companions, so we might expect that the visual binary MF would tend to be relatively higher than the spectroscopic MF. We caution that the large number of companions found in the WDS may result partially from the inclusion of field stars or cluster members that may or may not be gravitationally bound to the target star. This problem increases at the long end of the log P distribution (largest separation systems) where the estimated orbital periods become a significant fraction of the stellar lifetime. If, for example, we replace the last two highly populated bins in Figure 4 with the average in the shorter period bins, then the total multiplicity fraction integrated over all period bins is 1.14, consistent will the idea that most massive stars have at least one companion.

A number of investigators have explored the binary star period distribution, with a particular emphasis on the shorter period systems ($P < 10$ days). Kiminki & Kobulnicky (2012) developed a Monte-Carlo approach to sample the intrinsic distributions of binary parameters in a way comparable to their extensive spectroscopic observations of the massive stars in the Cyg OB2 association. They used a power-law distribution for orbital period of the form $f(\log P) \propto (\log P)^\beta$, and their experiments suggest $\beta = +0.2 \pm 0.4$, consistent with a flat distribution with $\beta = 0$ (Öpik's law). On the other hand, Sana et al. (2013b) used a similar Monte-Carlo method to fit spectroscopic results for a large sample of O-type stars in the Tarantula Nebula region of the LMC, and they find a best fit power-law distribution with $\beta = -0.45 \pm 0.30$. Their result is consistent with that from an analysis of Milky Way eclipsing binaries by Moe & Di Stefano (2013), who find $\beta = -0.4 \pm 0.3$. However, we caution that the distribution of shorter period systems may be more complicated and include a local maximum in numbers for periods in the range of 4–10 days (Barbá et al. 2010; Kiminki & Kobulnicky 2012; Sana et al. 2013b), so that a multi-component model is more appropriate than a single power law (Sana & Evans 2011). Our results (Figure 4) suggest that the distribution in log P is approximately flat when we consider the full range in orbital periods.

6. CONCLUSIONS

Our FGS survey has provided us with a new and uniform sample of high angular resolution observations to explore the
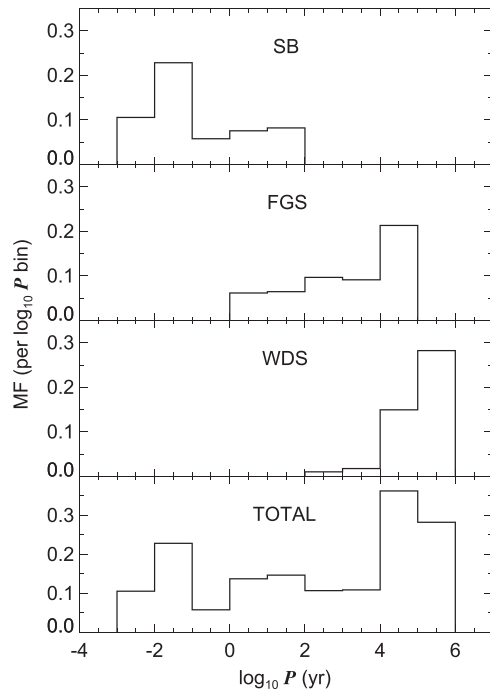
Figure 4. Histograms of the multiplicity fraction (MF) plotted as a function of orbital period. From top to bottom, successive panels show the distributions for the spectroscopic binary (SB), Fine Guidance Sensor (FGS), Washington Double Star (WDS), and total samples, respectively.

multiple star properties of massive stars in the projected separation range from $0\rlap{.}''01$ to $1\rlap{.}''0$ for companions brighter than $\triangle m = 5$ mag. We used detection techniques developed by Caballero-Nieves et al. (2014) to identify both faint companions and those close to the angular resolution limit. In total, we detected 59 binary systems and 6 triple systems among our sample of 224 stars, yielding a frequency of multiple systems of 29%. Of the 13 LBV or LBV candidates observed, 6 are found to have companions. Many of the resolved binaries also have one component that is a spectroscopic binary, so our results will help in the interpretation of their composite spectra. For example, all three of the bright stars BD+00°1617 A,B,C that line up in the center of the cluster Bochum 2 are resolved binaries, and two of these (B and C) are also short-period spectroscopic binaries (Munari & Tomasella 1999), forming hierarchies like those observed in the Orion Trapezium cluster (Close et al. 2012). Although most of the resolved binaries are distant and the projected separations imply a large semimajor axis, we do find a number of relatively nearby systems with close companions with probable orbital periods less than one century (including HD 155913, HD 158186, HDE 229232, HDE 303308, HD 160529, HD 164794 and HD 195592). These will be important targets for long-term observation for orbital and mass determinations.

We considered the binary star census of the complete sample (301 stars = 224 stars from this work less 4 LMC stars plus an additional 81 stars from earlier FGS studies) by collecting information from the literature on the numbers of close spectroscopic binaries and by searching the WDS Catalog for additional companions with angular separations mostly greater than 1 arcsec. The number of companions was compared between the spectroscopic (SB) and resolved (FGS, WDS) samples to determine the frequency of multiple systems and the companion frequency among stars residing in clusters and associations and in the field, and among runaway stars. These statistics for the SB and FGS samples confirm the trend that stars close to their place of birth have relatively more companions, consistent with the idea that stars ejected from clusters are preferentially single objects. The number of wide companions in the WDS sample may be overestimated because of the inclusion of cluster members and chance alignment cases rather than bound companions. The total number of companions per target among cluster and association stars falls in the range from 0.7 to 1.7 depending upon the inclusion of suspected spectroscopic binaries and the WDS companions.

We investigated the period distribution of the known binaries in this sample by collecting measured orbital periods for spectroscopic binaries and by estimating the periods for resolved binaries from their projected separation, distance, and probable mass. We constructed a histogram of the multiplicity frequency as a function of $\log P$ by accounting for the probable range in detectable period for each target that was set by the duration of the observations for spectroscopic binaries and by the angular separation range associated with the FGS and WDS measurements for the visual binaries. The resulting distribution is approximately flat over nine decades in $\log P$, consistent with Öpik's law. However, there remain some significant observational selection effects that may eventually alter this conclusion. Detailed spectroscopic and high angular resolution studies of massive stars in specific clusters with known distances will be particularly helpful in assessing the importance of such selection effects and determining the complete binary properties of a young massive star population (see Kiminki & Kobulnicky 2012; Sana et al. 2013b).

APPENDIX
NOTES ON INDIVIDUAL STARS

024044.94+611656.1 = HD 16429. McSwain (2003) found that the spectrum is a composite of an SB1 system and constant

velocity component. We assumed that one of these is the angularly resolved companion for counting purposes.

025107.97+602503.9 = HD 17505. The companion is resolved on the *y*-axis only and is far off-axis along the *x* direction. The results are consistent with the separation 2″15 and position angle 92°7 found by Maíz Apellániz (2010), although our estimated magnitude difference is slightly larger. Sota et al. (2011) obtained resolved spectra of both components and found that both are O-type stars. Note that component A of this pair is itself a spectroscopic triple star system (Hillwig et al. 2006).

040751.39+621948.4 = HD 25639 = SZ Cam. Resolved on both axes for the first observation (at a position consistent with that found by Balega et al. 2007), but only resolved along the *y*-axis in the second observation. We adopted the magnitude difference from the first observation and the second derivative amplitude a_x to estimate $|\triangle x|$ for the second observation. Gorda et al. (2007) show that the system consists of a short-period eclipsing binary with a distant companion that is probably also a binary (making the system a hierarchical quadruple). We assumed that the resolved component CHR 209 Ea,Eb is this second system for counting purposes.

051618.15 + 341844.3 = HD 34078. We did not detect the close ($\rho = 0″35$) companion of AE Aur discovered by Turner et al. (2008; TRN 17 Aa,Ab), which may have been an artifact of their AO observations (see Section 4).

051756.06–691603.9 = HDE 269321. This close pair is resolved along the *y*-axis only in both of our closely spaced observations.

051814.36–691501.1 = HD 35343 = S Dor. The companion is beyond the *x*-axis scan range in the second (short scan) observation.

053051.48–690258.6 = HDE 269662. The companion is close, faint, and detected along the *y*-axis only in two closely spaced observations.

053522.90–052457.8 = HD 37041A = θ² Ori A. The CHR 249 Aa,Ab pair is clearly resolved in the first observation, but in the second short scan observation the companion is beyond the scan range in *x* and is only partially resolved in the *y* direction.

062715.78+145321.2 = HD 45314. Mason et al. (1998) used speckle interferometry to resolve this target as a binary with a separation of 0″054 (named CHR 251 AB), but it was not resolved again in subsequent speckle observations (Mason et al. 2009). It appears single in the FGS scans.

064548.70–071839.0 = ALS85. This is a triple system where components B and C are comparable in brightness. Consequently, the correspondence between the components observed in both axes is ambiguous. Table 2 lists the result where the closer component is assumed to be B in both cases. If B has the larger projected separation in the *y*-axis scan, then the result for A,B is $\theta = 219°87 \pm 0°18$ and $\rho = 0″3378 \pm 0″0013$ and the result for A,C is $\theta = 233°29 \pm 0°20$ and $\rho = 0″3117 \pm 0″0011$.

071842.49 − 245715.8 = HD 57061. τ CMa is a multiple system with two components revealed by the FGS observations. The wider component was detected along both axes in the first observation, but only along the *x*-axis in the second observation. There is a low-amplitude peak in the cross correlation function for the second observation near the expected projected separation ($\triangle y \approx +0.19$) but it is below the adopted detection threshold. The system consists of a long-

period SB1 and a short-period eclipsing system (van Leeuwen & van Genderen 1997; Stickland et al. 1998), and we assumed that these two correspond to the bright resolved pair FIN 313 Aa,Ab. The WDS currently identifies Ab as the brighter of the two central objects, so we subtracted 180° in position angle and changed the sign of $\triangle m$ to make our results consistent with the others in the WDS for the Aa,Ab pair. The wider component Ab,E appears in the WDS with a 180° difference in position angle, but a reassessment of AstraLux Lucky Imaging observations by Maíz Apellániz (2010) indicates a placement consistent with the FGS results.

075220.28–262546.7 = HD 64315. This system was resolved as a binary by Mason et al. (2009) and named WSI 54 AB. Recent observations by Hartkopf et al. (2012) agree with the position angle and separation estimated from the FGS observations (Table 2). However, speckle observations by Tokovinin et al. (2010) suggest that the system may consist of a triple in a linear configuration, and hence our binary measurements may correspond to the center of light of the two companions. The fit of the *x*-axis scan with two components is marginal, but experiments with three component fits made little or no improvement, so we present the binary results in Table 2 for simplicity. Lorenzo et al. (2010) present a spectroscopic study and argue that the system consists of one SB2 system with a period of $P = 2.71$ days plus one SBE system with a period of 1.018 days. We assumed that each of these correspond to components of the resolved binary for counting purposes.

081517.15–354414.6 = CD-35 4384. This is a triple system with an inner companion Ab detected by FGS. It was difficult to rectify the low frequency trends in these long scans (particularly for the *x*-axis) and the magnitude difference for the wide pair Aa,B is taken from the *y*-axis result. Note that the actual uncertainty in magnitude difference may be larger than quoted in Table 2, because we do not account for spatial photometric sensitivity variations that become significant for widely separated systems.

081903.90–360844.9 = CD-35 4471. The companion was resolved along the *y*-axis only, but the second derivative test was nearly met for the *x*-axis result. Thus, we estimated $|\triangle x|$ from the *y*-axis magnitude difference and second derivative amplitude a_x. The result given in Table 2 corresponds to an assumed position at $+\triangle x$; for a projected position of $-\triangle x$, the position angle is $\theta = 146°4 \pm 6°1$.

084351.09–460346.5 = CD-45 4462. The FGS scans reveal this as a triple system. All three components appear in the *y*-axis scan, but the central pair is blended together in the *x*-axis scan. However, the second derivative amplitude is quite large for the central blend, so we estimated $|\triangle x|$ from the *y*-axis magnitude difference and second derivative amplitude a_x. Table 2 lists the position angle of A,B for $+\triangle x$, and the position angle for $-\triangle x$ is $\theta = 20°0 \pm 3°3$. All the magnitude differences are from the *y*-scan results.

085322.01–460208.8 = CD-45 4676. The B companion is resolved along the *y*-axis and blended with the central fringe along the *x*-axis. The second derivative test criterion is met in the latter case, so we estimated $|\triangle x|$ from the *y*-axis magnitude difference and second derivative amplitude a_x. The position angle for $+\triangle x$ is given in Table 2, and that for $-\triangle x$ is $\theta = 342°31 \pm 0°09$.

090221.56–484154.4 = CD-48 4352. This target appears as a triple in the *y*-axis scan and appears single in the *x*-axis scan.

However, the central fringe in the *x*-axis scan passes the second derivative test, and we assume that the implied fringe broadening is due only to the closer and brighter B component (i.e., that the wider and fainter C component falls beyond the recorded *x*-axis scan). Then we estimated $|\triangle x|$ from the *y*-axis magnitude difference and second derivative amplitude a_x. The $+|\triangle x|$ solution is used for the position angle in Table 2, and the result for $-|\triangle x|$ is $\theta = 18.6 \pm 2.9$.

100639.88–572533.1 = CPD-56 2853. The faint companion is resolved along the *y*-axis only. In this case the projected separation $(\triangle y = 0.''2)$ is wide enough that we cannot say whether or not the the companion is blended or off-scan along the *x*-axis, and consequently we simply present a lower limit for the separation in Table 2.

104505.85–594006.4 = HDE 303308. This target was detected as a close binary in earlier FGS observations by Nelan et al. (2004, 2010) with $\theta = 122° \pm 32°$ and $\rho = 0.''015 \pm 0.''002$ (resolved on the *y*-axis only). We obtained two additional observations that do not resolve the system. However, the second derivative test was suggestive of a companion (reaching a S/N of 3.3 for the *y*-axis scan of the second observation, but still below our detection criterion of S/N >4). Taking the second derivative amplitudes at their face values yields the minimum separations and position angles given in Table 3. Note that solution $^a\theta_2$ in the first observation is consistent with $^a\theta_1$ in the second observation. The fact that three independent observations all yield similar binary parameters indicates that this system is probably a long-period wide binary. The spectroscopic status is controversial. Chini et al. (2012) found the star to be radial velocity constant in 10 observations. On the other hand, Levato et al. (1991) measured one very low radial velocity over an eight-night run, consistent with a short-period eccentric binary orbit. Consequently, we label the spectroscopic status as "SB1?" in Table 1.

164120.41–484546.6 = HD 150136. The companion resolved in *x* only is consistent in position and magnitude difference with the known A,B pair. A companion with $\rho = 0.''0073$ detected in VLTI Amber observations by Sanchez-Bermudez (2013) is too close to be resolved in the FGS data. Sana et al. (2013a) discuss the orbits of the close binary and third star, and we include their period estimates in the spectroscopic category for Figure 4.

172912.93–313203.4 = HD 158186. A companion is detected along the *y*-axis only. We adopt $\triangle x = 0$ in Table 2.

181512.97–202316.7 = HD 167263. The close pair of 16 Sgr (CHR255 Aa,Ab) was observed in 3 previous speckle measurements with a position angle difference of 180° from the FGS results, but this is not unexpected for stars of similar brightness.

181805.90–121433.3 = HD 167971. De Becker et al. (2012) resolved this system with the VLTI and argued that it has an orbital period $P > 20$ yr. However, the separation was about 9 mas in 2008, which was too close for resolution with the somewhat noisier FGS scans we obtained. It is a hierarchical triple system with a close central binary.

182119.55–162226.1 = HD 168625. This target appears triple in the *x*-scans but double in the *y*-scan. It is not clear which of the two components in the *x*-scan corresponds to the single component in the *y*-scan, but we assumed that the component B with the smaller projected separation along the *x*-axis corresponds to the resolved component along the *y*-axis (and that component C falls beyond the range recorded for the

y-scan). The magnitude differences are taken from the *x*-axis data. The central fringe appeared somewhat asymmetrical in both *x* and *y* compared to those for the calibrator stars. Note that in the long scans made after 2009.1 (like this case) we often observe a weak feature at $\triangle x = -1.''2$ that has a systematic origin and should not be confused with a faint companion. Only companion B is recorded along the *x*-axis in the second, short scan observation. Component B is probably the companion detected in VLT-NACO observations by Martayan et al. (2012).

200329.40+360130.5 = HD 190429. Long scans were made to detect the signal of the wide B component. There are a few reports of a closer and fainter companion MCA 59 Aa,Ab at a separation of $\approx 0.''1$ (most recently by Mason et al. 1998). However, this close companion is not detected in the FGS scans.

201806.99+404355.5 = HD 193322A. This is a remarkable multiple system that is the subject of a detailed study with the CHARA Array long baseline interferometer by ten Brummelaar et al. (2011). The FGS observations resolve the Aa,Ab pair along the *y*-axis, but the pair is blended in the *x*-axis scan. A blend is indicated by the second derivative test and we used the *y*-scan magnitude difference and second derivative amplitude to find $|\triangle x|$. The solution using $-|\triangle x|$ is listed in Table 2, and the separation and position angle estimates agree well with contemporaneous CHARA array measurements (ten Brummelaar et al. 2011).

201851.71+381646.5 = HD 193443A. This system appears in the WDS with the brighter component identified as B, so we added 180° to the position angle and changed the sign of $\triangle m$ for consistency with the results in the WDS.

213857.62+572920.5 = HD 206267. This pair is resolved along the *y*-axis only, but the projected separation and magnitude difference are consistent with those for the known MIU 2 Aa,Ab system if the projected separation is small along the *x*-axis. The results in Table 2 assume $\triangle x = 0$. The system is an hierarchical triple (Stickland 1995; Burkholder et al. 1997), and we assumed that the resolved companion is the third star identified in the spectrum.

REFERENCES

Balega, I. I., Balega, Y. Y., Maksimov, A. F., et al. 2007, AstBu, 62, 339
Balona, L., & Crampton, D. 1974, MNRAS, 166, 203
Barbá, R. H., Gamen, R., Arias, J. I., et al. 2010, RMxAA, 38, 30
Bate, M. R. 2012, MNRAS, 419, 3115
Bonnell, I. A., & Bate, M. R. 2005, MNRAS, 362, 915
Bonnell, I. A., & Smith, R. J. 2011, in IAU Symp. 270, Computational Star Formation, ed. J. Alves, B. G. Elmegreen, J. M. Girart, & V. Trimble (Cambridge: Cambridge Univ. Press), 57
Brandeker, A., Jayawardhana, R., Khavari, P., Haisch, K. E. Jr., & Mardones, D. 2006, ApJ, 652, 1572
Burkholder, V., Massey, P., & Morrell, N. 1997, ApJ, 490, 328
Caballero-Nieves, S. M. 2012, PhD thesis, Georgia State Univ.
Caballero-Nieves, S. M., Nelan, E. P., Gies, D. R., et al. 2014, AJ, 147, 40
Cameron, E. 2011, PASA, 28, 128
Chini, R., Hoffmeister, V. H., Nasseri, A., Stahl, O., & Zinnecker, H. 2012, MNRAS, 424, 1925
Close, L. M., Puglisi, A., Males, J. R., et al. 2012, ApJ, 749, 180
Correia, S., Zinnecker, H., Ratzka, T., & Sterzik, M. F. 2006, A&A, 459, 909
Cruz-González, C., Recillas-Cruz, E., Costero, R., Peimbert, M., & Torres-Peimbert, S. 1974, RMxAA, 1, 211
Cvetković, Z., Vince, I., & Ninković, S. 2010, NewA, 15, 302
De Becker, M., Rauw, G., & Linder, N. 2009, ApJ, 704, 964
De Becker, M., Sana, H., Absil, O., le Bouquin, J.-B., & Blomme, R. 2012, MNRAS, 423, 2711
de Wit, W. J., Testi, L., Palla, F., & Zinnecker, H. 2005, A&A, 437, 247

Duchêne, G., & Kraus, A. 2013, ARA&A, 51, 269
Garmany, C. D., Conti, P. S., & Chiosi, C. 1982, ApJ, 263, 777
Garmany, C. D., Conti, P. S., & Massey, P. 1980, ApJ, 242, 1063
Gorda, S. Y., Balega, Y. Y., Pluzhnik, E. A., & Shkhagosheva, Z. U. 2007, AstBu, 62, 352
Gualandris, A., Portegies Zwart, S., & Eggleton, P. P. 2004, MNRAS, 350, 615
Gudennavar, S. B., Bubbly, S. G., Preethi, K., & Murthy, J. 2012, ApJS, 199, 8
Hartkopf, W. I., & Mason, B. D. 2004, RMxAA, 21, 83
Hartkopf, W. I., Tokovinin, A., & Mason, B. D. 2012, AJ, 143, 42
Hillwig, T. C., Gies, D. R., Bagnuolo, W. G. Jr., et al. 2006, ApJ, 639, 1069
Horch, E. P., Franz, O. G., Wasserman, L. H., & Heasley, J. N. 2006, AJ, 132, 836
Humphreys, R. M. 1978, ApJS, 38, 309
Kaczmarek, T., Olczak, C., & Pfalzner, S. 2011, A&A, 528, A144
Kiminki, D. C., & Kobulnicky, H. A. 2012, ApJ, 751, 4
Kobulnicky, H. A., Smullen, R. A., Kiminki, D. C., et al. 2012, ApJ, 756, 50
Kratter, K. M., Matzner, C. D., & Krumholz, M. R. 2008, ApJ, 681, 375
Kraus, S., Weigelt, G., Balega, Y. Y., et al. 2009, A&A, 497, 195
Krumholz, M. R., Klein, R. I., McKee, C. F., Offner, S. S. R., & Cunningham, A. J. 2009, Sci, 323, 754
Kuiper, R., & Yorke, H. W. 2013, ApJ, 772, 61
Lafrenière, D., Jayawardhana, R., van Kerkwijk, M. H., Brandeker, A., & Janson, M. 2014, ApJ, 785, 47
Larson, R. B. 2010, RPPh, 73, 014901
Levato, H., Malaroda, S., Morrell, N., Garcia, B., & Hernandez, C. 1991, ApJS, 75, 869
Lorenzo, J., Simón-Díaz, S., Negueruela, I., & Vilardell, F. 2010, in ASP Conf. Ser. 435, Binaries—Key to Comprehension of the Universe, ed. A. Prša, & M. Zejda (San Francisco: ASP), 409
Maíz Apellániz, J. 2010, A&A, 518, A1
Maíz-Apellániz, J., Walborn, N. R., Galué, H. Á., & Wei, L. H. 2004, ApJS, 151, 103
Maíz Apellániz, J., Sota, A., Morrell, N. I., et al. 2013, in Massive Stars: From Alpha to Omega, arXiv:1306.6417
Markwardt, C. B. 2009, in ASP Conf. Ser. 411, Astronomical Data Analysis Software and Systems XVIII, ed. D. A. Bohlender, D. Durand, & P. Dowler (San Francisco, CA: ASP), 251
Martayan, C., Lobel, A., Baade, D., et al. 2012, in ASP Conf. Ser. 464, Circumstellar Dynamics at High Resolution, ed. A. C. Carciofi, & T. Rivinius (San Francisco, CA: ASP), 293
Martins, F., Schaerer, D., & Hillier, D. J. 2005, A&A, 436, 1049
Mason, B. D., Gies, D. R., Hartkopf, W. I., et al. 1998, AJ, 115, 821
Mason, B. D., Hartkopf, W. I., Gies, D. R., Henry, T. J., & Helsel, J. W. 2009, AJ, 137, 3358
Mason, B. D., Wycoff, G. L., Hartkopf, W. I., Douglass, G. G., & Worley, C. E. 2001, AJ, 122, 3466
Matt, S., & Pudritz, R. E. 2008, ApJ, 681, 391
McSwain, M. V. 2003, ApJ, 595, 1124

McSwain, M. V., Boyajian, T. S., Grundstrom, E. D., & Gies, D. R. 2007, ApJ, 655, 473
Mel'Nik, A. M., & Dambis, A. K. 2009, MNRAS, 400, 518
Mermilliod, J.-C., & Mermilliod, M. 1994, in Catalogue of Mean UBV Data on Stars (Berlin: Springer)
Moe, M., & Di Stefano, R. 2013, ApJ, 778, 95
Moffat, A. F. J., Jackson, P. D., & Fitzgerald, M. P. 1979, A&AS, 38, 197
Munari, U., & Tomasella, L. 1999, A&A, 343, 806
Nazé, Y., Vreux, J.-M., & Rauw, G. 2001, A&A, 372, 195
Nelan, E., Younger, J., Makidon, R. B., et al. 2014, Fine Guidance Sensor Instrument Handbook for Cycle 22 v.21.0 (Baltimore: STSI)
Nelan, E. P., Walborn, N. R., Wallace, D. J., et al. 2004, AJ, 128, 323
Nelan, E. P., Walborn, N. R., Wallace, D. J., et al. 2010, AJ, 139, 2714
Perryman, M. A. C., & ESA (ed.) 1997, Proc. of the ESA Symposium. The HIPPARCOS and TYCHO Catalogues (ESA SP-1200; Paris: ESA)
Peter, D., Feldt, M., Henning, T., & Hormuth, F. 2012, A&A, 538, A74
Pickles, A., & Depagne, É. 2010, PASP, 122, 1437
Raghavan, D., McAlister, H. A., Henry, T. J., et al. 2010, ApJS, 190, 1
Rauch, T., Heber, U., Hunger, K., Werner, K., & Neckel, T. 1991, A&A, 241, 457
Richardson, N. D., Gies, D. R., Morrison, N. D., et al. 2012, in ASP Conf. Ser. 465, Proc. of a Scientific Meeting in Honor of Anthony F. J. Moffat, ed. L. Drissen, C. Robert, N. St-Louis, & A. F. J. Moffat (San Francisco, CA: ASP), 160
Sana, H., & Evans, C. J. 2011, in IAU Symp. 272, Active OB Stars: Structure, Evolution, Mass Loss, and Critical Limits, ed. C. Neiner, G. Wade, G. Meynet, & G. Peters (Cambridge: Cambridge Univ. Press), 474
Sana, H., Le Bouquin, J.-B., De Becker, M., et al. 2011, ApJL, 740, L43
Sana, H., Le Bouquin, J.-B., & Mahy, L. 2013, A&A, 553, A131
Sana, H., de Mink, S. E., de Koter, A., et al. 2012, Sci, 337, 444
Sana, H., de Koter, A., de Mink, S. E., et al. 2013, A&A, 550, A107
Sana, H., Le Bouquin, J.-B., Lacour, S., et al. 2015, ApJS, 215, 15
Sanchez-Bermudez, J., Schödel, R., Alberdi, A., et al. 2013, A&A, 554, L4
Sota, A., Maíz Apellániz, J., Morrell, N. I., et al. 2014, ApJS, 211, 10
Sota, A., Maíz Apellániz, J., Walborn, N. R., et al. 2011, ApJS, 193, 24
Stickland, D. J. 1995, Obs, 115, 180
Stickland, D. J. 1997, Obs, 117, 37
Stickland, D. J., Lloyd, C., & Sweet, I. 1998, Obs, 118, 7
ten Brummelaar, T. A., O'Brien, D. P., Mason, B. D., et al. 2011, AJ, 142, 21
Tokovinin, A., Mason, B. D., & Hartkopf, W. I. 2010, AJ, 139, 743
Turner, N. H., ten Brummelaar, T. A., Roberts, L. C., et al. 2008, AJ, 136, 554
van Genderen, A. M. 2001, A&A, 366, 508
van Leeuwen, F., & van Genderen, A. M. 1997, A&A, 327, 1070
Wegner, W. 1994, MNRAS, 270, 229
Williams, S. J., Gies, D. R., Hillwig, T. C., McSwain, M. V., & Huang, W. 2011, AJ, 142, 146
Zacharias, N., Finch, C. T., Girard, T. M., et al. 2013, AJ, 145, 44
Zinnecker, H., & Yorke, H. W. 2007, ARA&A, 45, 481